IET Renewable Power Generation

Research Article

IET Journals
The Institution of Engineering and Technology

Towards robust OPF solution strategy for the future AC/DC grids: case of VSC-HVDC-connected offshore wind farms

ISSN 1752-1416
Received on 31st August 2017
Revised 18th January 2018
Accepted on 26th January 2018
E-First on 20th February 2018
doi: 10.1049/iet-rpg.2017.0575
www.ietdl.org

Ahmad Nikoobakht[1], Jamshid Aghaei[2,3] ✉, Taher Niknam[2], Vahid Vahidinasab[4], Hossein Farahmand[3], Magnus Korpås[3]

[1]*Higher Education Center of Eghlid, Eghlid, Iran*
[2]*Department of Electrical and Electronics Engineering, Shiraz University of Technology, Shiraz, Iran*
[3]*Department of Electric Power Engineering, Norwegian University of Science and Technology (NTNU), Trondheim NO-7491, Norway*
[4]*Department of Electrical Engineering, Abbaspour School of Engineering, Shahid Beheshti University, Tehran, Iran*
✉ *E-mail: aghaei@sutech.ac.ir*

Abstract: This study jointly addresses two major challenges in power system operations: (i) sustained growth of intermittent offshore wind farms (OWFs) connected to AC grid via multi-terminal voltage source converter (VSC)-based high-voltage DC (HVDC) grid that brings new challenges to the power system operation, and (ii) dealing with non-linearity of the AC power flow equations with the multi-terminal VSC-based HVDC grid model. To overcome these challenges, firstly, to deal with the uncertainties caused by the high penetration of the intermittent OWFs, this study introduces a robust optimisation approach. The proposed framework is computationally efficient and does not require the probability density function of the wind speed. The proposed decision-making framework finds the optimal decision variables in a way that they remain robust against the set of uncertainties. Secondly, the mathematical representation of the full AC optimal power flow (OPF) problem, with the added modelling of multi-terminal VSC-based HVDC grid in a day-ahead scheduling problem, is a mixed-integer non-linear programming (MINLP) optimisation problem, which is computationally burdensome for large-scale systems. Accordingly, this paper proposes a computationally efficient method for adjustment of solutions set points, which is also compatible with existing customary solvers with minimal modification efforts.

Nomenclature

Indices

g	index for generating units
$n, n'/m, m'$	indices for system buses
k/l	index for line
ℓ	index for angle piece
t	index related to time period

Sets

χ_n	set of thermal units which are connected to bus n
Ω_n	set of lines which are connected to bus n
$\Omega_{n'}^{\mathrm{DC}}$	set of buses with HVDC lines

Continuous variables

$\delta_{nmt}^{(\cdot)}$	phase angle difference across line (n, m) at period t
$\omega_{n't}$	amplitude modulation ratio in VSC-HVDC
$P_{gt}^{(\cdot)}/Q_{gt}^{(\cdot)}$	active/reactive power output of thermal unit g at period t
$V_{nt}^{(\cdot)}/V_{n't}^{\mathrm{dc}}$	voltage magnitude for HVAC/DC at bus n/n' at period t
$P_{nmt}^{(\cdot)}/Q_{nmt}^{(\cdot)}$	active/reactive power flow on line (n, m)
$P_{nm}(\ell)/Q_{nm}(\ell)$	active/reactive power flow on the ℓth linear block of line (n, m)
$P_{nm}^{(\cdot)}(\ell, i)/Q_{nm}^{(\cdot)}(\ell, i)$	active/reactive power flow on the ℓth/ith linear block/breakpoint of line (n, m)
$\bar{\Delta}P_{gt}^{(\cdot)}/\underline{\Delta}P_{gt}^{(\cdot)}$	active power increase/decrease in thermal unit g for security purposes
Q_{nt}^{dc}	reactive power flowing into HVDC link
$R_{n'm'}$	resistance of HVDC cable
$x_{nn'l}$	reactance of HVDC coupling transformer
TC	total system operation cost Note that the normal condition $s = 0$ relate to the first stage

Binary variables

$u_{mn}(\ell)$	status of the ℓth linear block of line (n, m)
u_{gt}	status of unit g at period t

Constants

$\delta_{nm}^{\max}$	max angle difference across a line (n, m)
$\bar{\delta}_{nm}(\ell)$	tangent point of the ℓth piecewise linear block of angle difference across a line (n, m)
$\alpha_{nm}(\ell)/\tilde{\alpha}_{nm}(\ell)$	slope of the ℓth piecewise linear block of the linearised $F(\delta_{nm}(\ell))/\tilde{F}(\delta_{nm}(\ell))$ relative to the line (n, m) in tangent point $\bar{\delta}_{nm}(\ell)$
$\beta_{nm}(\ell)/\tilde{\beta}_{nm}(\ell)$	value of the linearised $F(\delta_{nm}(\ell))/\tilde{F}(\delta_{nm}(\ell))$ relative to the ℓth piecewise linear block-of-the line (n, m) in tangent point $\bar{\delta}_{nm}(\ell)$
$\alpha_{nm}(\ell, i)/\tilde{\alpha}_{nm}(\ell, i)$	slope of the ℓ/ith piecewise linear block/breakpoint of the linearised $F(\bar{\delta}_{nm}(\ell), g(i), b(i))/\tilde{F}(\bar{\delta}_{nm}(\ell), g(i), b(i))$ relative to the line (n, m) with TCSC device
$\beta_{nm}(\ell, i)/\tilde{\beta}_{nm}(\ell, i)$	value of the linearised $F(\bar{\delta}_{nm}(\ell), g(i), b(i))/\tilde{F}(\bar{\delta}_{nm}(\ell), g(i), b(i))$ relative to the ℓ/ith piecewise linear block/breakpoint of the line (n, m) with TCSC device
$C_g/C_g^{\pm}$	cost of normal/stress condition of thermal unit g
$S_k^{\max}$	maximum magnitude of apparent power of line k, MVA

ψ_{D_n}	power factor angle of load n
$\Delta R_g^{\pm}$	ramp up/down limit of unit g at stress condition
$Q_g^{\max}/Q_g^{\min}$	max/min reactive power output of unit g
PD_{nt}/QD_{nt}	active/reactive power demand of load n at period t
$\mathrm{SU}_{gt}/\mathrm{SD}_{gt}$	start-up/shutdown cost of unit g
$\Delta\delta$	length of each piecewise linear block, in radians
M	disjunctive factor, a large positive value
g_k	conductance of line k, a non-negative value
b_k/b_{k0}	series/shunt admittance of line k, a negative value
Δ_g^{LAC}	active power generation calculation error for linear ACOPF model for unit g
$\Delta_{mn}^{\mathrm{LAC}}$	active power flow calculation error for linear ACOPF model in line (n, m)

1 Introduction

The application of wind power generation, especially offshore wind farms (OWFs), is a keystone in the policy of several countries for high penetration of renewable energy resources. In many countries, the best location for onshore wind farms are already developed and the utilities are turning to offshore sites. The main reason for this attraction is the availability of enormous wind resources [1]. There are many advantages associated with OWFs as follows: (i) with OWFs, noise and visual impacts are eliminated and besides, the environmental impact is significantly reduced, allowing the designers of the wind turbines to produce larger wind turbines with longer blades that can effectively produce more electricity [2]. (ii) The OWFs take the advantages of the stronger and more constant winds that exist in the sea. As a result, the OWFs' generation are more efficient and more reliable, they can produce more electricity and they can maintain higher levels of electricity generation for longer periods of time [1, 2]. The main disadvantage of the OWFs is generally that they are located far away from the onshore grid. Provided that the distance is long or if the OWF is connected to a weak AC onshore grid, a high-voltage DC (HVDC) transmission system may be a more suitable choice than the conventional high-voltage AC (HVAC) transmission network [1]. Nowadays, more and more large-scale OWFs are getting integrated into the system through HVDC transmission lines due to the limitation of traditional HVAC lines. Two types of HVDC transmission topologies, i.e. HVDC with voltage source converter (VSC-HVDC) using insulated gate bipolar transistors (IGBTs) and line-commutated converter HVDC (LCC-HVDC) are used today for OWFs connectivity [3, 4]. The OWFs integration by conventional LCC HVDC system and full-bridge diode rectifier-based HVDC is studied in [4]. However, the little voltage or reactive support can be provided to the main grid by the OWFs due to the uncontrollability of such HVDC systems [4]. Nevertheless, the VSC-based HVDC lines utilising full-controllable components such as IGBT or GTO can enable AC voltage support to the connected HVAC system by the OWFs. Also, in comparison with the conventional LCC-HVDC systems, VSC-HVDC systems show many advantages. These include the independent control of reactive and active power, continuous AC voltage regulation, no commutation failure, no voltage polarity reversal needed to reverse power, black-start capability, compact filters, and lighter cables [3, 4], ability to control the negative sequence current injection in the OWF outputs [5], shorter design, and installation times [6]. Both of these HVDC technologies have their own cons and pros and choosing the best technology for HVDC link depends on the requirements of the planner, which is not the subject of this work. There have been great advances in the practical VSC-HVDC techniques. Several VSC stations (multi-terminal systems) can be connected to DC buses with fixed polarity, creating DC grids similar to AC networks. These VSC-HVDC grids are very attractive for OWFs integration and the reinforcement of interconnected AC networks [1]. Therefore, the number of multi-terminal systems, which feed power to an AC network at different points, is increasing. As a result, the interest in studying the performance of such systems has been increasing. Many projects have investigated the potential benefits and cost-effectiveness of the multi-terminal VSC-HDVC, as well as its impact on the security of the connected AC networks and the need of the coordination of power control at the multiple DC links [1, 7, 8]. Such multi-terminal VSC-HDVC systems are also well suited for connection of OWFs to onshore AC grids. This is the reason that in [9], multi-terminal VSC-HDVC systems have been introduced as a cost-effective solution to connect OWFs to the onshore AC systems. There are many practical reasons proving that the VSCs are more suitable for building such multi-terminal HDVC systems. In contrast to the LCC, VSCs not only have no reactive power demand but can also regulate the reactive power to maintain AC-side voltage as a generator [3].

Multi-terminal VSC-HDVC systems with parallel-connected converters have a great potential to be used in the future bulk power systems [10]. Also, over the past few years, significant studies have been done to address the different challenges associated with the operation and control of converters in the HVDC transmission as well as broadening its applications [11–13]. These references present robust control technique for stable operation of converters in the HVDC transmission systems.

The possibility of such connections has led to the proposition of a DC 'SuperGrid' that could connect several OWFs to a common multi-terminal DC grid [14]. On the other hand, lack of smart grid management strategies for operation of HDVC and HVAC grids can result in uninvited outcomes such as congestion on transmission systems and decreasing the power grid efficiency [7, 14]. Furthermore, the role of the transmission congestion in smart power networks has been addressed in [12]. In this work, a novel routing economic dispatch algorithm has been presented for congestion management of smart power system. Similarly, high penetration of OWFs could decrease the operation cost and reduction in peak-time demand, whereas its uncertainty could impose adverse effects on system congestion [9, 14]. In this way, multi-terminal VSC-HVDC systems mitigate the intermittency of wind generation and enhance system reliability as well as reduce transmission congestion. Thus, this paper investigates the utilisation of the multi-terminal VSC-HVDC to facilitate a higher utilisation of the OWFs generation, during the wind uncertainty. Besides, in [9, 14], the multi-terminal VSC-HDVC systems have been included in the DC optimal power flow problem (DCOPF). Accordingly, the mathematical representation of the DCOPF, with the added modelling of multi-terminal VSC-HDVC systems, is a non-linear programme (NLP). These references present a method to convert this NLP into a linear problem. It is worth mentioning that coordination of the multi-terminal VSC-HDVC systems with HVAC grid based on DCOPF cannot consider ACOPF feasibility, which hinders the exploitation of the benefits of the HVDC lines in power system operations. Unfortunately, deployment of the multi-terminal VSC-HVDC systems is limited today due to the complexities that these systems introduce to the HVAC systems. Besides, optimal adjustment of the multi-terminal VSC-HVDC systems with HVAC grids introduces mixed-integer non-linear programming (MINLP) in the day-ahead scheduling problem; hence, employing an MINLP solver does not guarantee to find a global optimum solution, especially when the scale of the problem is large [14, 15]. Such an optimisation problem with the above-mentioned multi-terminal VSC-HVDC lines is called precise OPF. Therefore, in order to overcome these challenges, in this paper, a linearised AC optimal power flow model as well as linearised multi-terminal VSC-HVDC models have been proposed; so, the proposed method convert this MINLP problem into a mixed-integer linear program (MILP) without loss of the model accuracy.

The aim of this paper is to cooperate the AC and DC systems for maximising variation range of OWFs generation uncertainty that the power system can accommodate for a given system congestion condition, while satisfying the technical constraints and system reliability. The problem of uncertainty modelling of the OWFs output is still an important issue [16]. In this paper, a new deterministic model is utilised for handling the OWFs output uncertainty. There is no need to the probability density function of wind speed and it is not computationally expensive compared to

Table 1 Taxonomy of our proposed model in the current paper

Refs	Year	Linear ACOPF (MILP)	Multi-terminal VSC-based HVDC grid (MILP)	Day-ahead scheduling problem (MILP)	Wind uncertainty (non-probabilistic/possibilistic (non-fuzzy) method)
[9]	2016	N	Y	Y	N
[14]	2015	N	Y	N	N
[20]	2016	Y	N	Y	N
[21, 22]	2016	N	N	Y	Y
[4]	2015	N	N	N	Y
[3]	2011	N	N	Y	N
[10]	2013	N	Y	N	N
[23]	2016	Y	N	N	N
current paper	—	Y	Y	Y	Y

Y/N denotes that the subject is/is not considered.

other uncertainty handling tools. The proposed decision-making structure finds the optimal decision variables in a way that they remain robust against the considered uncertainties.

The available literatures, which attempted the uncertainty modelling of the wind power in day-ahead scheduling problems, can be classified as follows: (i) stochastic methods [17], (ii) fuzzy uncertainty modelling methods [17, 18], and (iii) robust optimisation (RO) [17]. Each method has its own pros and cons. For instance, the main disadvantage of the stochastic methods is the requirement for accurate statistical models of uncertain parameters [17]. It is usually computationally expensive and adds huge execution burden to the original problem. The fuzzy programming requires the membership function for the wind power uncertainty modelling [18]. It is usually difficult to extract a true fuzzy numbers and they should be mapped into real valued numbers. The RO approach needs to know the variation range of the wind uncertain parameters (WUPs) and the lower and upper level of WUPs are fixed before solving the problem [17, 19]. The proposed approach of this paper for the uncertainty modelling of the OWFs' output is both non-possibilistic (non-fuzzy) and non-probabilistic and does not require to predefine variation range of the WUPs. Challenges related to high uncertainty of the OWFs output in the power system can be managed with optimal adjustment of the HVDC and HVAC grids. The coordination of these grids that allows revising operation decisions closer to real time can, indeed, mitigate the impact of the OWFs output uncertainty. In the technical literature, there are few works addressing the co-operation of the multi-terminal VSC-HVDC grids with HVAC grids in a day-ahead scheduling problem. In [9, 14], a co-operation of HVDC lines with HVAC grid in an AC OPF problem is proposed. Note that wind power uncertainty is not modelled either in [9, 14]. Finally, Table 1 shows the taxonomy of the proposed day-ahead scheduling problem with incorporating linear multi-terminal VSC-HVDC system in to a linear ACOPF model, in previous literatures.

Considering the above discussion, the main contributions of this work with respect to the previous references in the literature include:

- Developing a linearised AC model incorporating linearised multi-terminal VSC-HVDC model in which bus voltage magnitudes and reactive power are taken into account. Based on this linearised AC model, a novel MILP formulation is recommended.
- Determining maximum variation range of the OWFs output uncertainty that a power system can accommodate for a given system congestion condition using simultaneously coordinated operation of HVAC and HVDC grids.
- A new non-probabilistic and non-possibilistic method is proposed for handling high penetration of the OWFs output uncertainty, which is specific to the current paper. The proposed robust optimisation technique guarantees the decision maker's objective function against the undesired severe effects of the OWFs output uncertainty in the proposed day-ahead scheduling problem.

To the best of the authors' knowledge, no research in the area has provided the MILP formulation for day-ahead scheduling problem with linearised AC OPF and multi-terminal VSC-HVDC system models in the presence of the high penetration of OWFs uncertainty.

The rest of the paper is organised as follows. Section 2 expresses the proposed linearisation of the AC power flow with multi-terminal VSC-HVDC model. Section 3 describes the proposed model of this paper. The proposed solution methodology is designated in Section 4. Section 5 demonstrates proposed case studies and the future work and main conclusions are highlighted in Sections 6 and 7.

2 Linearisation of the full AC power flow with multi-terminal VSC-HVDC model

This section presents a linear approximation to AC power flow in which voltage and reactive power are modelled. The linearisation idea is founded on a piecewise linear (PWL) approximation and the following assumptions are assumed to be valid: (i) the bus voltage scales are continuously nearly to 1.0 per unit (p.u.), (ii) the angle difference through a transmission line is small, i.e. $\delta_{nm} \simeq 0 - 34^{\circ}$.

2.1 Linearisation of the AC power flow equations

The active and reactive AC power flow in transmission line k between buses n and m are written as follows:

$$P_{nm} = g_k V_n^2 - V_n V_m \overbrace{(g_k \cos\delta_{nm} + b_k \sin\delta_{nm})}^{F(\delta_{nm})} \tag{1a}$$

$$Q_{nm} = -(b_k + b_{k0})V_n^2 + V_n V_m \overbrace{(b_k \cos\delta_{nm} - g_k \sin\delta_{nm})}^{\tilde{F}(\delta_{nm})} \tag{1b}$$

where $F(\delta_{nm})$ and $\tilde{F}(\delta_{nm})$ are non-linear functions. Assume, also they have local convexity within the specific interval, e.g. $\underline{\delta}_{nm} < \delta_{nm} < \bar{\delta}_{nm}$. One can represent $F(\delta_{nm})$ and $\tilde{F}(\delta_{nm})$ using a PWL functions as did in [24], with $2L$ pieces (as shown in Fig. 1). It is noted that the illustrated curves in Figs. 1*a* and *b* show the typical form of functions $F(\delta_{nm})$ and $\tilde{F}(\delta_{nm})$ based on the real values of b_k and g_k in the real transmission networks. The convex approximation of the $F(\delta_{nm})$ and $\tilde{F}(\delta_{nm})$ functions are implemented through a PWL function that produces a linear formulation in the following way. As shown in Fig. 1, the linear approximation of the $F(\delta_{nm})$ and $\tilde{F}(\delta_{nm})$ in the range of $[-L, L]$ can be obtained using $2L$ piece PWL approximation. Accordingly, ℓth piece function for each line (n, m) through the tangent point (i.e. $\bar{\delta}_{nm}(\ell)$) is obtained as follows:

$$\forall\delta_{nm} \in [(-L-1+\ell)\Delta\delta, (-L+\ell)\Delta\delta], \ell = 1, \ldots, 2LF(\delta_{nm}) = \alpha_{nm}(\ell)\left(\delta_{nm} - \bar{\delta}_{nm}(\ell)\right) + \beta_{nm}(\ell), \tag{1c}$$

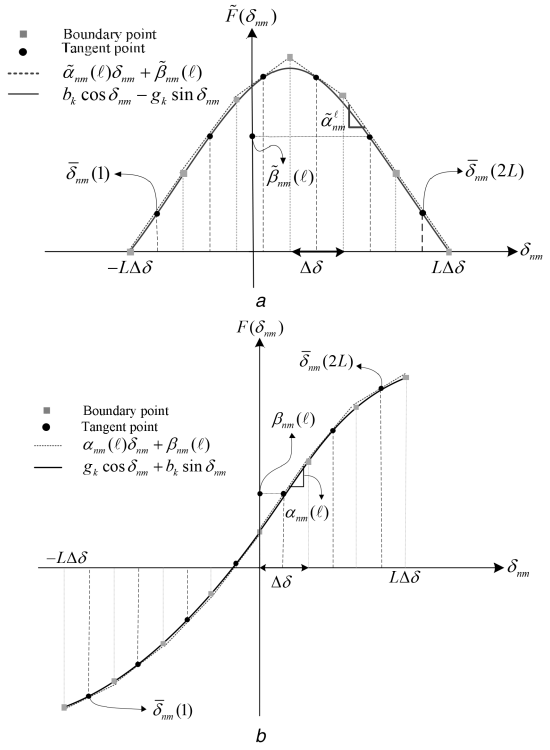

Fig. 1 *Illustration of piecewise-linear linearization for functions*
(a, b) The piecewise-linear approximation of $\tilde{F}(\delta_{nm})$ and $F(\delta_{nm})$ using $2L$ piece equalities, respectively

Table 2 Approximation errors in line flow terms (voltages and angle in p.u. and radian, respectively)

Term	Range of operation	Approximation	Max abs error
V_n^2	$0.95 \le V_n \le 1.05$	$2V_n - 1$	0.0025
V_nV_m	$0.95 \le V_{n/m} \le 1.05$	$V_n + V_m - 1$	0.0025
$V_nV_m\delta_{nm}$	$0.95 \le V_{n/m} \le 1.05$ and $\delta_{nm} \simeq \bar{\delta}_{nm}(\ell)$	$\bar{\delta}_{nm}(\ell)(V_n + V_m - 1) + (\delta_{nm} - \bar{\delta}_{nm}(\ell))$	0.0050
$\omega_{n'}V_{n'}V_n$	$0.95 \le V_{n/n'} \le 1.05$ and $0.9 \le \omega_{n'} \le 1.1$	$V_n + V_{n'} + \omega_{n'} - 2$	0.0025
$\omega_{n'}V_{n'}^{\mathrm{dc}}V_n\delta_{nn'}$	$0.95 \le V_n \le 1.05$, $0.9 \le V_{n'}^{\mathrm{dc}} \le 1.1$, $\omega_{n'} \simeq \omega_{n'}^0$ and $\delta_{nn'} \simeq \delta_{nn'}^0$	$V_{n'}^{\mathrm{dc}^0}V_n^0\delta_{nn'}^0\left(\omega_{n'} - \omega_{n'}^0\right) + \omega_{n'}^0V_n^0\delta_{nn'}^0\left(V_{n'}^{\mathrm{dc}} - V_{n'}^{\mathrm{dc}^0}\right)$ $+\omega_{n'}^0V_{n'}^{\mathrm{dc}^0}\delta_{nn'}^0\left(V_n - V_n^0\right) + \omega_{n'}^0V_{n'}^{\mathrm{dc}^0}V_n^0\left(\delta_{nn'} - \delta_{nn'}^0\right) + \omega_{n'}^0V_{n'}^{\mathrm{dc}^0}V_n^0\delta_{nn'}^0$	0.005

$$\forall\delta_{nm} \in [(-L-1+\ell)\Delta\delta, (-L+\ell)\Delta\delta],\ \ell = 1, \ldots, 2L\tilde{F}(\delta_{nm}) = \tilde{\alpha}_{nm}(\ell)\left(\delta_{nm} - \bar{\delta}_{nm}(\ell)\right) + \tilde{\beta}_{nm}(\ell) \quad (1d)$$

where $\alpha_{nm}(\ell)$ and $\tilde{\alpha}_{nm}(\ell)$ are the slope of each linear piece, at tangent point (i.e. $\bar{\delta}_{nm}(\ell)$), for the $F(\delta_{nm})$ and $\tilde{F}(\delta_{nm})$, respectively. Besides, $\beta_{nm}(\ell)$ and $\tilde{\beta}_{nm}(\ell)$ are the values of the $F(\delta_{nm})$ and $\tilde{F}(\delta_{nm})$ at the tangent point (i.e. $\bar{\delta}_{nm}(\ell)$) for each linear piece, respectively. Note that, the execution of (1c) and (1d) for the PWL model of $F(\delta_{nm})$ and $\tilde{F}(\delta_{nm})$ requires either binary variables or special ordered sets of type 2 (SOS-2) [25]. Finally, the parameters $\alpha_{nm}(\ell)$, $\tilde{\alpha}_{nm}(\ell)$ $\beta_{nm}(\ell)$, and $\tilde{\beta}_{nm}(\ell)$ are obtained by the below equations

$$\alpha_{nm}(\ell) = \frac{\partial\tilde{F}}{\partial\delta_{nm}}\left(\delta_{nm} - \bar{\delta}_{nm}(\ell)\right)$$
$$\tilde{\alpha}_{nm}(\ell) = \frac{\partial\tilde{F}}{\partial\delta_{nm}}\left(\delta_{nm} - \bar{\delta}_{nm}(\ell)\right) \quad (1e)$$

$$\beta_{nm}(\ell) = F\left(\delta_{nm} - \bar{\delta}_{nm}(\ell)\right)$$
$$\tilde{\beta}_{nm}(\ell) = \tilde{F}\left(\delta_{nm} - \bar{\delta}_{nm}(\ell)\right) \quad (1f)$$

where $\bar{\delta}_{nm}(\ell) = ((-L-1+\ell)\Delta\delta + (-L+\ell)\Delta\delta/2)$.

Substituting (1c) and (1d) into (1a) and (1b), then the following equations:

$$\begin{aligned} P_{nm}(\ell) &\simeq g_kV_n^2 - V_nV_m\left[\alpha_{nm}(\ell)\left(\delta_{nm} - \bar{\delta}_{nm}(\ell)\right) + \beta_{nm}(\ell)\right] \\ &= g_kV_n^2 - V_nV_m\alpha_{nm}(\ell)\delta_{nm} \\ &\quad + V_nV_m\alpha_{nm}(\ell)\bar{\delta}_{nm}(\ell) - V_nV_m\beta_{nm}(\ell) \end{aligned} \quad (1g)$$

$$\begin{aligned} Q_{nm}(\ell) &\simeq -(b_k + b_{k0})V_n^2 + V_nV_m\left[\begin{array}{l}\tilde{\alpha}^{\ell}_{nm}\left(\delta_{nm} - \bar{\delta}_{nm}(\ell)\right) \\ +\tilde{\beta}_{nm}(\ell)\end{array}\right] \\ &= -(b_k + b_{k0})V_n^2 + V_nV_m\tilde{\alpha}_{nm}(\ell)\delta_{nm} \\ &\quad - V_nV_m\tilde{\alpha}_{nm}(\ell)\bar{\delta}_{nm}(\ell) + V_nV_m\tilde{\beta}_{nm}(\ell) \end{aligned} \quad (1h)$$

Notice that (1g) and (1h) still contain some non-linear terms like V_nV_m, $V_nV_m\delta_{nm}$, and V_n^2. These non-linear terms can be linearised by their Taylor series expansion around 1, for bus voltage, and about $\bar{\delta}_{nm}(\ell)$, for transmission line angle, as presented in Table 2.

Table 2 gives the maximum absolute errors for each of the constituent terms with respect to the linearised forms, over a typical range of operating voltages and angles, i.e. $0.95 \le V_n \le 1.05$ at the end of each line, and $|\delta_{nm}| \le 34^{\circ}$. Subsequently, the PWL approximation of active and reactive AC power flow equations for line (n, m) metered at bus n for ℓth angle piece (or through the tangent point, i.e. $\bar{\delta}_{nm}(\ell)$) are obtained as follows, respectively:

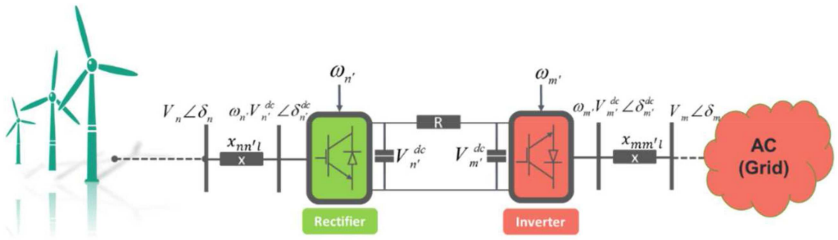

Fig. 2 *Schematic diagram of OWFs connected via the VSC-HVDC transmission link*

$$P_{nm}(\ell) = g_k(2V_n - 1) - \alpha_{nm}(\ell)\left[\delta_{nm} - \bar{\delta}_{nm}(\ell)\right] - \beta_{nm}(\ell)(V_n + V_m - 1) \tag{1i}$$

$$Q_{nm}(\ell) = -(b_k + b_{k0})(2V_n - 1) + \tilde{\alpha}_{nm}(\ell)\left[\delta_{nm} - \bar{\delta}_{nm}(\ell)\right] + \tilde{\beta}_{nm}(\ell)(V_n + V_m - 1) \tag{1j}$$

The above-mentioned formulations, i.e. (1) and (2), are valid for each segment of the δ_{nm} (where $(-L-1+\ell)\Delta\delta < \delta_{nm} < (-L+\ell)\Delta\delta$, $\ell \in [-L, L]$), or close to each tangent point (i.e. $\bar{\delta}_{nm}(\ell)$), as shown in Fig. 1.

Note that the length of each segment of angle is $\Delta\delta$ (as shown in Fig. 1). More details about piecewise linearisation can be found in [24]. It essentially introduces $2L$ new binary variables and $2L$ new inequalities, all being linear. To ensure which segment of the PWL blocks is selected, a binary variable $u_{nm}(\ell)$ is used as follows:

$$(-L-1+\ell)\Delta\delta - M(1-u_{nm}(\ell)) < \delta_{nm}\delta_{nm} < (-L+\ell)\Delta\delta + M(1-u_{nm}(\ell)) \tag{2a}$$

$$\sum_{\ell} u_{nm}(\ell) = 1 \tag{2b}$$

Note that, each angle difference across a line (n, m) metered at bus n only can be placed on one linear piece as done by (2b), where, the active or reactive line flows for line (n, m) metered at bus n are obtained as follows:

$$\forall k \in (n,m) \quad P_{nm}(\ell) - M(1-u_{nm}(\ell)) \le P_{nm} \le P_{nm}(\ell) + M(1-u_{nm}(\ell)) \tag{2c}$$

$$Q_{nm}(\ell) - M(1-u_{nm}(\ell)) \le Q_{nm} \le Q_{nm}(\ell) + M(1-u_{nm}(\ell)) \tag{2d}$$

Here, $u_{nm}(\ell)$is a binary variable, and M is a sufficiently large positive scalar. However, adding the binary variables (especially, in constraint (2c)) is likely to complicate the resultant model and makes it inefficient once the problem is implemented for a large-scale system. For this reason, if (1i) approximated with one block angel at zero tangent point (i.e. $\bar{\delta}_{nm}(\ell) = 0$), then (1i) becomes a convex equation and no binary variable is needed. Accordingly, the constraint (2c) could be removed from the problem. In addition, by this action, the proposed model can be relaxed to make trade-off between the model accuracy and the computation time.

2.2 Linearisation of the multi-terminal VSC-HVDC equations

In the case of the multi-terminal VSC-HVDC grid, the full formulation for the power flow between nodes (n, n') and (n', m') is given by (3). As can be seen in Fig. 2, the lines between nodes (n, n') and (n', m') are modelled as series impedance and resistance, respectively.

In (3), $P^{dc}_{nn'l}$ and $Q^{dc}_{nn'l}$ are active and reactive power flows at transmission line l between buses n and m

$$P^{dc}_{nn'l} = \left(\frac{\omega_{n'} V^{dc}_{n'} V_n}{x_{nn'l}}\right) \mathrm{Sin}\left(\delta_n - \delta^{dc}_{n'}\right), \quad \delta_n - \delta^{dc}_{n'} = \delta_{nn'} \tag{3a}$$

$$Q^{dc}_{nn'l} = \frac{V_n\left(V_n - \omega_{n'} V_{n'} Cos\left(\delta_n - \delta^{dc}_{n'}\right)\right)}{x_{nn'l}} \tag{3b}$$

$$P^{dc}_{nn'l} = \sum_{m'} \frac{V^{dc}_{n'}\left(V^{dc}_{n'} - V^{dc}_{m'}\right)}{R_{n'm'}} \tag{3c}$$

where $\sum_{m'}$ is the set of lines connected to bus n'.

To maintain the system security, it is assumed that $\delta_{nn'}$ for each bus n and n' which are connected by line $l(n, n')$ is small enough and voltage magnitude is ∼1 p.u. for these buses. These assumptions are practically true under normal operating condition. On the basis of these assumptions, it is proposed to rewrite (3) by replacing sine and cosine functions with their Taylor series expansion about zero, so that $\sin(\delta_n - \delta^{dc}_{n'}) \simeq \delta_n - \delta^{dc}_{n'}$ and $\cos\left(\delta_n - \delta^{dc}_{n'}\right) \simeq 1$ can be applied, and also by substituting quadratic function of V^2_n, two-variable function of $V^{dc}_{n'}V_n$, $V^{dc}_{n'}V^{dc}_{m'}$, three-variable function of $\omega_{n'}V_{n'}V_n$, and four-variable function of $\omega_{n'}V^{dc}_{n'}V_n\delta_{nn'}$ with their Taylor series expansion about $\omega^0_{n'}$, $V^{dc^0}_{n'}$, V^0_n, and $\delta^0_{nn'}$, as presented in Table 2. Finally, based on the assumptions above, the linearisation of the multi-terminal VSC-HVDC line power flow (3a)–(3c) can be written as follows:

$$\begin{aligned} P^{dc}_{nn'l} &= \left(\frac{\omega_{n'} V^{dc}_{n'} V_n}{x_{nn'l}}\right) \mathrm{Sin}(\delta_{nn'}) \simeq \left(\frac{1}{x_{nn'l}}\right)\left(\omega_{n'} V^{dc}_{n'} V_n \delta_{nn'}\right) \\ &\simeq \frac{1}{x_{nn'l}} \begin{pmatrix} V^{dc^0}_{n'} V^0_n \delta^0_{nn'}\left(\omega_{n'} - \omega^0_{n'}\right) + \omega^0_{n'} V^0_n \delta^0_{nn'}\left(V^{dc}_{n'} - V^{dc^0}_{n'}\right) \\ +\omega^0_{n'} V^{dc^0}_{n'} \delta^0_{nn'}\left(V_n - V^0_n\right) + \omega^0_{n'} V^{dc^0}_{n'} V^0_n\left(\delta_{nn'} - \delta^0_{nn'}\right) \\ +\omega^0_{n'} V^{dc^0}_{n'} V^0_n \delta^0_{nn'} \end{pmatrix} \end{aligned} \tag{3d}$$

$$\begin{aligned} Q^{dc}_{nn'l} &= \frac{V_n(V_n - \omega_{n'} V_{n'} Cos(\delta_{nn'}))}{x_{nn'l}} \\ &\simeq \frac{\left(V^2_n - \omega_{n'} V_{n'} V_n\right)}{x_{nn'l}} \simeq \frac{(V_n - \omega_{n'} - V_{n'} + 1)}{x_{nn'l}} \end{aligned} \tag{3e}$$

$$\begin{aligned} P^{dc}_{nn'l} &= \sum_{m'} \frac{V^{dc}_{n'}\left(V^{dc}_{n'} - V^{dc}_{m'}\right)}{R_{n'm'}} \\ &\simeq \sum_{m'} \frac{\left(V^{dc^2}_{n'} - V^{dc}_{n'} V^{dc}_{m'}\right)}{R_{n'm'}} \simeq \sum_{m'} \frac{\left(V^{dc}_{n'} - V^{dc}_{m'}\right)}{R_{n'm'}} \end{aligned} \tag{3f}$$

2.3 Model description

This section describes in detail all constraints used in the proposed robust day-ahead scheduling problem incorporating linearised multi-terminal VSC-HVDC model. Accordingly, the proposed formulation for day-ahead scheduling problem with multi-terminal VSC-HVDC system is addressed in the following subsections by (4) and (5). In these formulations, the total cost (TC) of the day-ahead scheduling problem is considered as the objective function as mentioned in (4a), which is subjected to the first- and second-stage constraints, (4) and (5), respectively

$$\min \ \mathrm{TC} = \sum_t \sum_g \begin{pmatrix} \left(C_g P^0_{gt} + \mathrm{SU}_{gt} + \mathrm{SD}_{gt}\right) \\ +C^{\pm}_g\left(\left(\underline{\Delta} P^+_{gt} + \bar{\Delta} P^+_{gt}\right) + \left(\underline{\Delta} P^-_{gt} + \bar{\Delta} P^-_{gt}\right)\right) \end{pmatrix} \tag{4a}$$

The objective function consists of two main parts: first-stage and second-stage parts. The first-stage part refers to offered generation

cost plus start-up and shutdown costs at the base case (normal condition) (i.e. $C_g P^0_{gt} + \mathrm{SU}_{gt} + \mathrm{SD}_{gt}$). Besides, the second-stage part mentions the cost of power adjustments for the *lower* and *upper* boundaries of possible OWF output uncertainty (i.e. $C^{\pm}_g\big(\underline{\Delta}P^{+}_{gt} + \bar{\Delta}P^{+}_{gt}\big)$ and $C^{\pm}_g\big(\underline{\Delta}P^{-}_{gt} + \bar{\Delta}P^{-}_{gt}\big)$ lower and upper boundaries of possible OWF output uncertainty, respectively), that ensures a secure operation in the admissible regions. In the admissible regions, the wind uncertainty can be fully admitted by additional emergency thermal units re-dispatch. On the other hand, if the actual wind uncertainty exceeds the admissibility boundaries and enters the inadmissible region, it may lead to undesired power imbalance that cannot be fully handled by the online thermal units re-dispatch. The part of forecasted OWF output uncertainty which is within the admissible region is admissible and riskless, while part that is out of the admissible region can lead to operational risk.

Subsequently, the first-stage constraints are:

$$u_{gt}P^{\min}_{g} \le P^{0}_{gt} \le u_{gt}P^{\max}_{g} \quad \forall g,t \tag{4b}$$

$$u_{gt}Q^{\min}_{g} \le Q^{0}_{gt} \le u_{gt}Q^{\max}_{g} \quad \forall g,t \tag{4c}$$

$$\sum_{g\in\chi_n} P^{0}_{gt} + \sum_{m\in\Omega_n} P^{0}_{nmt} + \sum_{n'\in\Omega_n} P^{\mathrm{dc}0}_{nn't} + \sum_{w\in\kappa_n} P^{\mathrm{for}}_{wt} = PD_{nt} \quad \forall n, t \tag{4d}$$

$$\sum_{g\in\chi_n} Q^{0}_{gt} + \sum_{m\in\Omega_n} Q^{0}_{nmt} + \sum_{n'\in\Omega_n} Q^{\mathrm{dc}0}_{nn't} = QD_{nt} = PD_{nt}\tan(\psi_{D_{nt}}) \quad \forall n,t \tag{4e}$$

$$\begin{cases} -P^{\max}_{k} \le P^{0}_{nmt} \le P^{\max}_{k} \\ -P^{\mathrm{dc}\min}_{k} \le P^{\mathrm{dc}0}_{nn't} \le P^{\mathrm{dc}\max}_{k} \end{cases} \quad \forall n,n',t,k \tag{4f}$$

$$\begin{cases} -Q^{\max}_{k} \le Q^{0}_{nmt} \le Q^{\max}_{k} \\ -Q^{\mathrm{dc}\min}_{k} \le Q^{\mathrm{dc}0}_{nn't} \le Q^{\mathrm{dc}\max}_{k} \end{cases} \quad \forall n,n',t,k \tag{4g}$$

$$\big(P^{0}_{nmt}\big)^2 + \big(Q^{0}_{nmt}\big)^2 \le \big(S^{\max}_{kt}\big)^2,\ \forall n,t,k \tag{4h}$$

$$\begin{cases} V^{\min}_{n} \le V_{nt} \le V^{\max}_{n},\ \forall n,t \\ V^{dc\min}_{n'} \le V^{dc}_{n't} \le V^{dc\max}_{n'},\ \forall n',t \end{cases} \tag{4i}$$

$$(1\mathrm{i}) - (1\mathrm{q}), (3\mathrm{d}) - (3\mathrm{f}) \tag{4j}$$

Constraints (4b) and (4c) force the limits of active and reactive power generation for thermal units, respectively. Constraints (4d) and (4e) denote the linearised active/reactive power balance in normal condition at each bus. The maximum active/reactive line flow capacity for HVAC transmission line k and HVDC transmission line $l(n,n')$ are defined by (4f) and (4g). In constraint (4h), since P^0_{nm} and Q^0_{nm} are linearised, the MVA limit for line k can be written as a second-order cone constraint. Notice that (4h) is still convex equation and can be handled by most commercial linear solvers such as Gurobi [26]. Nevertheless, if a solver requires the constraint to be *strictly* linear, a piecewise linearised version for (4h) can also be derived [23]. Bus voltage magnitude limits for HVAC and HVDC transmission lines are ensured by (4i). Constraint (4j) corresponds to power flow equations related to HVAC and HVDC transmission lines that host multi-terminal VSC-HVDC system.

The second-stage constraints are:

$$P^{\pm}_{gt} = \Big(P^{0}_{gt} + \big(\bar{\Delta}P^{+}_{gt} - \underline{\Delta}P^{+}_{gt}\big) + \big(\bar{\Delta}P^{-}_{gt} - \underline{\Delta}P^{-}_{gt}\big)\Big) \quad \forall g,t \tag{5a}$$

$$u_{gt}Q^{\min}_{g} \le Q^{\pm}_{gt} \le u_{gt}Q^{\max}_{g} \quad \forall g,t \tag{5b}$$

$$\forall n,t,k \in (n,m) \sum_{g\in\chi_n} P^{\pm}_{gt} + \sum_{m\in\Omega_n} P^{\pm}_{nmt} + \sum_{n'\in\Omega_n} P^{\mathrm{dc}\pm}_{nn't} + (1\pm\alpha)P^{\mathrm{for}}_{wt} = PD_{nt} \tag{5c}$$

$$\sum_{g\in\chi_n} Q^{\pm}_{gt} + \sum_{m\in\Omega_n} Q^{\pm}_{nmt} + \sum_{n'\in\Omega_n} Q^{\mathrm{dc}\pm}_{nn't} = PD_{nt}\cdot\tan(\psi_{D_{nt}}) \tag{5d}$$

$$\begin{cases} -P^{\max}_{k} \le P^{\pm}_{nmt} \le P^{\max}_{k} \\ -P^{\mathrm{dc}\min}_{k} \le P^{\mathrm{dc}\pm}_{nn't} \le P^{\mathrm{dc}\max}_{k} \end{cases} \quad \forall n,n',t,k \tag{5e}$$

$$\begin{cases} -Q^{\max}_{k} \le Q^{\pm}_{nmt} \le Q^{\max}_{k} \\ -Q^{\mathrm{dc}\min}_{k} \le Q^{\mathrm{dc}\pm}_{nn't} \le Q^{\mathrm{dc}\max}_{k} \end{cases} \quad \forall n,n',t,k \tag{5f}$$

$$\big(P^{\pm}_{nmt}\big)^2 + \big(Q^{\pm}_{nmt}\big)^2 \le \big(S^{\max}_{k}\big)^2,\ \forall n,t,k \in (n,m) \tag{5g}$$

$$\begin{cases} V^{\min}_{n} \le V^{\pm}_{nt} \le V^{\max}_{n},\ \ \forall n,t \\ V^{\mathrm{dc}\min}_{n'} \le V^{\mathrm{dc}\pm}_{n't} \le V^{\mathrm{dc}\max}_{n'},\ \ \forall n',t \end{cases} \tag{5h}$$

$$(1\mathrm{i}) - (1\mathrm{q}), (3\mathrm{d}) - (3\mathrm{f}) \tag{5i}$$

$$\big|P^{0}_{gt} - P^{\pm}_{gt}\big| \le \Delta R^{\pm}_{g},\ \forall g \tag{5j}$$

where '$\pm$' in (5): '$-$' and '$+$' refer to the *lower* and *upper* boundaries of possible wind uncertainty, respectively. Constraint (5a) links between the normal and lower/upper wind uncertainty conditions that thermal units to enforce corrective actions by up/down re-dispatch of thermal units adjustments, i.e. $\bar{\Delta}P^{\pm}_{gt}/\underline{\Delta}P^{\pm}_{gt}$. Constraint (5b) is similar to (4c), but it is for lower/upper wind uncertainty conditions. The power flow equations for the lower/upper OWF output uncertainty condition are specified by (5c) and (5d). A scalar variable lower/upper wind uncertainty margin $\pm\alpha$ is an arbitrary choice to force upper, $(+\alpha)$, and lower, $(-\alpha)$, wind uncertainty, respectively. The constraints (5f)–(5i) have the same expressions as (4f)–(4i), respectively, where the variables P^0_{gt}, Q^0_{gt}, P^0_{nmt}, Q^0_{nmt}, $Q^{\mathrm{dc}0}_{nn't}$, $V^{\mathrm{dc}0}_{n't}$, and V^0_{nt} are replaced by $P^{\pm}_{gt}$, $Q^{\pm}_{gt}$, $P^{\pm}_{nmt}$, $Q^{\pm}_{nmt}$, $Q^{\mathrm{dc}\pm}_{nn't}$, $V^{\mathrm{dc}\pm}_{n't}$, and $V^{\pm}_{nt}$, respectively. The changes in the generation of thermal units are limited by ramp constraint as mentioned in (5j). The $\Delta R^{\pm}_{g}$ represents physically the acceptable adjustments of power output of thermal units in 10 min (i.e. 10/60 of hourly ramping of thermal units) to guarantee the desired security margin.

3 OWF uncertainty model

With the proposed model above, the independent system operator can examine the admissibility of wind power generation, consequently determine the admissible region of OWF output under the given robust day-ahead scheduling strategy. It is worthy to note that, besides the robust day-ahead scheduling strategy, the system congestion also remarkably influences the admissibility of OWF output, since the admissible OWF output can vary among different network congestion. In this regard, here hosted multi-terminal VSC-HVDC system to eliminate system congestion and maximise the size of admissible regions of the OWF outputs comparable in the conventional HVAC systems. Then, the admissibility assessment problem is converted into a robust optimisation problem, where by the admissible region of the OWF outputs can be determined reasonably. As shown in Fig. 3, obviously, the upper and lower boundaries of possible maximum admissible regions of the OWF outputs are the $(1+\alpha^{\max})P^{\mathrm{for}}_{wt}$ and $(1-\alpha^{\max})P^{\mathrm{for}}_{wt}$, respectively. Noted that, the maximum admissible regions of the OWF outputs occur in the $\mathrm{TC}^{\max}$, namely the maximum TC of the robust day-ahead scheduling problem. This constitutes the space of maximum possible deviation of actual realisation of the OWF uncertain parameter from its forecasted value. Assuming regions wind power uncertainty have been

obtained, the space of OWF output uncertainty can be divided into two parts by the admissibility (grey arrow) and inadmissibility (red arrow) boundaries, respectively. In the admissible region, no additional emergency regulation is required since any arbitrary realisation of OWF outputs can be fully admitted without breaking the operational feasibility. On the other hand, if the actual OWF outputs exceeds the admissibility boundaries and enters the inadmissible region, it may lead to undesired power imbalance that cannot be fully handled by the committed thermal units themselves. In such a situation, additional emergency regulations, such as fast-ramping units and/or reducing the share of OWF to supply load, may have to be used to recover the operation feasibility. Also, one way to increase the admissible region in power system operation is reducing network congestion by implementing multi-terminal VSC-HVDC system in HVAC grid.

The OWF output uncertainty level considered ranges from zero to one in such a way that α uncertainty means that the *upper* and *lower* boundaries of possible OWF output uncertainty are equal to the OWF output forecast multiplied by $(1+\alpha)$ and $(1-\alpha)$, respectively.

To derive the robust day-ahead scheduling problem with OWF output uncertainty, we want to obtain the largest variation range of the OWF output uncertainty that the system can accommodate, or maximum admissible regions of the OWF outputs, with multi-terminal VSC-HVDC system. The largest variation range of the OWFs output from its forecasted value can formulated as follows:

$$\max \quad \alpha \tag{6a}$$

$$\overbrace{\sum_t \sum_g \left(C_g P^0_{gt} + C^{\pm}_g \left(\begin{matrix} \left(\underline{\Delta} P^{+}_{gt} + \bar{\Delta} P^{+}_{gt}\right) \\ +\left(\underline{\Delta} P^{-}_{gt} + \bar{\Delta} P^{-}_{gt}\right) \end{matrix} \right) \right)}^{\mathrm{TC}} \le (1+\xi)\mathrm{TC}_b \tag{6b}$$

The first-stage constraints are:

$$(4a)\,\text{to}\,(4j) \tag{6c}$$

The second-stage constraints are:

$$(5a)\,\text{to}\,(5j) \tag{6d}$$

The objective function (6a) of the above problem is to maximise the boundaries of the admissibility of OWF output uncertainty. Equation (6b) indicates that the cost of the corrective actions must not exceed the cost threshold for any realisation of uncertainty.

4 Solution methodology

The robust day-ahead scheduling model with multi-terminal VSC-HVDC system in (6) is a large-scale, non-convex, non-deterministic polynomial-time hard (NP-hard) problem. The corresponding solution for large-scale systems would be an intractable task without decomposition.

The Benders decomposition (BD) is adopted to decompose the proposed problem into a master problem and several tractable subproblems [27]. Fig. 4 shows the flowchart of the solution methodology based on the BD technique. Detail formulations of Benders' master problem and subproblems are provided in Fig. 4.

4.1 Master problem

The master problem resultant to the original robust day-ahead scheduling problem with multi-terminal VSC-HVDC system is formulated as an MILP problem (7). The objective function (7a) corresponds to (6a)

$$\max \quad \alpha \tag{7a}$$

$$(4b), (5b), (5j) \tag{7b}$$

$$\sum_g P^0_{gt} + P^{\mathrm{for}}_{wt} = PD_{nt} \quad \forall n \tag{7c}$$

$$\sum_g P^{\pm}_{gt} + (1 \pm \alpha) P^{\mathrm{for}}_{wt} = PD_{nt} \quad \forall n \tag{7d}$$

Constraint (7b) comprises the first- and second-stage constraints, which are mentioned in Section 2. The system load balances for the first and second stage are given in (7c) and (7d), respectively.

4.2 Subproblem

The subproblem is formulated in (8):

$$\text{Min } Z = \sum_n \left((MP^0_{1,nt} + MP^0_{2,nt}) + (MP^{\pm}_{1,nt} + MP^{\pm}_{2,nt}) \right) \tag{8a}$$

$$\begin{aligned} &\forall n,t,k \in (n,m) \sum_{g \in \chi_n} P^0_{gt} + \sum_{m \in \Omega_n} P^0_{nmt} + \sum_{m \in \Omega_n} P^{dc^0}_{nmt} + P^{\mathrm{for}}_{wt} \\ &= PD_{nt} + MP^0_{1,nt} + MP^0_{2,nt} \end{aligned} \tag{8b}$$

$$\left(\begin{matrix} \sum_{g \in \chi_n} P^{\pm}_{gt} + \sum_{m \in \Omega_n} P^{\pm}_{nmt} \\ + \sum_{m \in \Omega_n} P^{dc^{\pm}}_{nmt} + (1 \pm \alpha) P^{\mathrm{for}}_{wt} \end{matrix} \right) = PD_{nt} + MP^{\pm}_{1,nt} + MP^{\pm}_{2,nt} \tag{8c}$$

$$(4d) - (4j)\,\text{and}\,(5c) - (5i) \tag{8d}$$

$$P^0_{gt} = \hat{P}^{0^{(v-1)}}_{gt} \rightarrow \mu^{(v-1)}_{gt} \tag{8e}$$

$$P^{\pm}_{gt} = \hat{P}^{\pm^{(v-1)}}_{gt} \rightarrow \mu^{\pm^{(v-1)}}_{gt} \tag{8f}$$

$$u_{gt} = \hat{u}^{(v-1)}_{gt} \rightarrow \eta^{(v-1)}_{gt} \tag{8g}$$

$$\alpha = \hat{\alpha}^{(v-1)} \rightarrow \gamma^{(v-1)} \tag{8h}$$

The hourly subproblem (8a) minimises slack variables $\left(MP^0_{1,nt}, MP^0_{2,nt}\right)$ and $\left(MP^{\pm}_{1,nt} + MP^{\pm}_{2,nt}\right)$ which represent the amount of active power mismatch for the first and second stage that should be added to corresponding buses to remove violations. The constraints (8b) and (8c) are similar to constraints (4d) and (5c), respectively, which are mentioned in Section 2. Constraint (8d) comprises transmission constraints for the first and second stage. Constraints (8e)–(8g) fix the values of the complicating variables to specified values achieved from the master problem solution. If the objective function (8a) is larger than zero, a Benders cut (8h) will be formed and added to master problem for calculating the next iterative solution of master problem. Besides, following each iteration of subproblem, the complicating variables are fixed through constraints (8e)–(8h), whose dual variables, $\mu^{(v-1)}_{gt}$, $\mu^{\pm^{(v-1)}}_{gt}$, $\eta^{(v-1)}_{gt}$, and $\gamma^{(v-1)}$ provide sensitivities to be applied in constructing Benders' cuts (8i) for feedback to the master problem

$$\begin{aligned} \hat{Z}^{(j)}_t + \sum_g \left(\begin{matrix} \mu^{(j)}_{gt}(P^0_{gt} - \hat{P}^{0^{(j)}}_{gt}) + \mu^{\pm^{(j)}}_{gt}(P^{\pm}_{gt} - \hat{P}^{\pm^{(j)}}_{gt}) \\ +\eta^{(j)}_{gt}(u_{gt} - \hat{u}^{(j)}_{gt}) \end{matrix} \right) \\ +\gamma^{(j)}(\alpha - \alpha^{(j)}) \le 0, \quad j = 1,2,\ldots,v-1 \end{aligned} \tag{8i}$$

The $\hat{Z}^{(j)}_t$ in Benders cuts corresponds to hourly bus power mismatches at each iteration of subproblem in BD approach. In this work, the Benders' cuts are functions of hourly scheduling variables such as hourly power dispatch of thermal units in the first and the second stages, hourly scheduling in the first stage and the maximum radius of the OWF output uncertainty. Actually, $\mu^{(v-1)}_{gt}$, $\mu^{\pm^{(v-1)}}_{gt}$, $\eta^{(v-1)}_{gt}$, and $\gamma^{(v-1)}$ demonstrate the sensitivity change of scheduling variables of the master problem solved from the previous iteration of subproblem. They help the master problem to recommend a better hourly scheduling and power dispatch of thermal units at the next iterations, that is, the master problem and subproblem be combined to each other by these cuts.

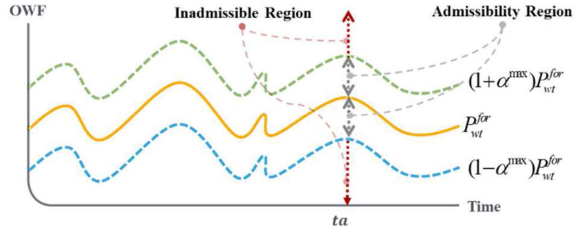

Fig. 3 *Schematic diagram of the proposed RO model*

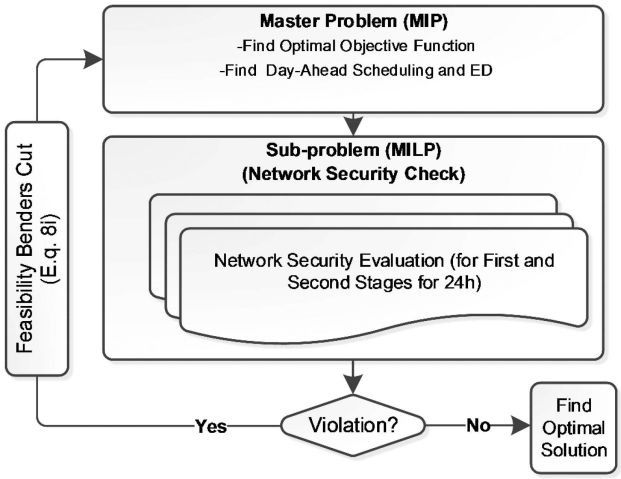

Fig. 4 *Solution strategy based on BD technique*

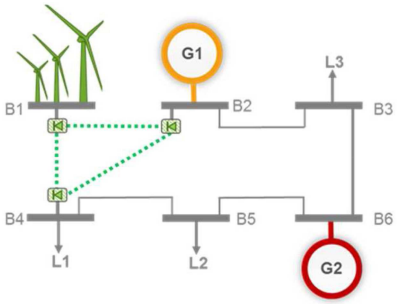

Fig. 5 *Modified six-bus test system with a three-terminal VSC-HVDC network*

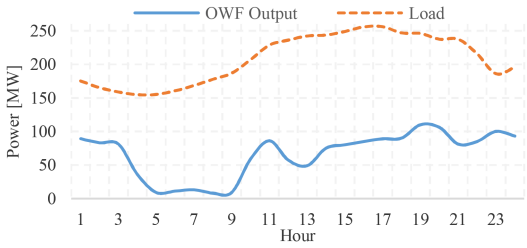

Fig. 6 *OWF forecast and system load profile*

5 Case study

A modified 6-bus test system along with and the IEEE 118-bus test system are used to analyse the proposed day-ahead scheduling problem with multi-terminal VSC-HVDC system. The proposed model has been formulated as an MILP problem, and it is solved using GAMS with CPLEX solver on an Intel i7, 8-core CPU at 3.40 GHz with 32 GB of RAM.

5.1 Modified six-bus system

The modified six-bus test system illustrated in Fig. 5 has two thermal units, seven transmission lines, and three load points. The thermal units from most expensive to cheapest are G1 and G2, respectively. The thermal units from low to high flexibility are *G*1 (lower ramping capability) and *G*2 (higher ramping capability), respectively. Besides, unit *G*2 is a fast-ramping unit with a 20 MW/(10 min) capacity, with a min/max power output of 10/20 MW, respectively. The lines flow limit for the lines 1–4, 2–3, and 4–5 are 86, 57, and 80 MVA, respectively, and 200 MVA for all other lines. The OWF unit with a maximum power output of 110 MW is installed at bus 1, which is ~43% of the system peak load. The percentage of available OWF output and load for each hour are given in Fig. 6.

To study the influence of multi-terminal VSC-HVDC system on the admissibility boundaries of the OWF output, the following two cases are tested:

Case 1: In this case, the day-ahead scheduling problem is optimally found in order to increase the admissibility boundaries of OWF output without multi-terminal VSC-HVDC system.

Case 2: The admissibility boundaries of OWF output in case 1 with AC/DC transmission constraints have been increased in which the AC line 1–2 and 1–4 and 2–4 are replaced with a multi-terminal VSC-HVDC transmission link as can be seen in Fig. 5.

The simulation results according to the mentioned case studies are presented as follows:

Case 1: As it was already explained, the first step, the day-ahead scheduling problem, i.e. (4) and (5), without multi-terminal VSC-HVDC system, has been solved to calculate the objective function of the base case for all 24 h, i.e. TC_b. It is assumed, for all 24 h, that the forecasted wind power is 100% of its installed capacity for OWF at bus 1. The TC of energy procurement including thermal unit generation (TUG) is equal to $TC_b = 78{,}698.52$ \$. At the second stage, the day-ahead scheduling problem (4) and (5) without multi-terminal VSC-HVDC system has been solved to obtained maximum admissibility boundaries of the OWF output uncertainty, i.e. α^{max}.

As shown in Table 3, the α^{max} value is 0.004; here, this obtained result is taken as the baseline of the comparisons. The resulting largest net OWF output variation range (the area between the red and blue curves) over the 24 h time horizon is too narrow, as shown in Fig. 7*a*. This matter may occur either due to transmission congestion (i.e. lines 1–2, 2–4, and 2–4) or thermal unit ramping limitations. Here, congestion in lines 1–2, 2–4, and 2–4 plays an important role in the maximum admissibility boundaries of the OWF output uncertainty. This is because of the OWF unit which is installed in bus 1, with more OWF output, the power through the lines connected to buses 1, 2, and 4 are increased. In this condition, power flowing through lines 1–2, 1–4, and 2–4 will be above their limits. For example, as shown in Table 4, the power flow at lines 1–4, 2–3, and 4–5 at hour 19 have been reached to their maximum capacity limits. In this condition, there will be transmission congestion remaining in the system that other transmission lines could not increase the flows to their limits. Also, in this case, the hourly OWF variations at bus 1 are more compensated by the up/down-ramping of inexpensive thermal units *G*1 at bus 2. On the other hand, these congestions caused that inexpensive *G*1 cannot increase/decrease its output in order to compensate variability of the OWF output at bus 1 and cannot satisfy the system load at peak hours. For this reason, in order to lower the power flowing on these congested lines and increase the ability of thermal unit *G*1 to accommodate OWF volatility, just one option is available, bringing a new unit on line in peak hours, therefore, bringing fast-ramping and expensive unit *G*2 is the best choice here, as shown in Table 3. In this condition, while the fast-ramping unit *G*2 is the only flexible option that follows the OWF uncertainty; accordingly, this unit is committed to provide a fast ramping capacity of 20 MW/(10 min) at hours 15–17 when there is an hourly OWF output increase. However, as the fast-ramping unit *G*2 is more expansive than thermal unit *G*1 in this system, this unit is turned off once the ramping flexibility is not required. The additional dispatch of expensive fast-ramping unit G2 at these hours would increase system operation costs and decrease admissibility boundaries of the OWF output. Also, as can be seen in Table 3, the cheaper unit *G*1 is on at all hours to accommodate the OWF volatility, while unit

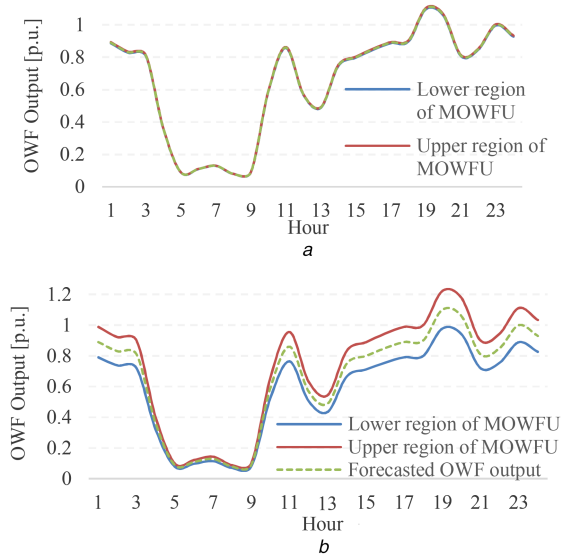

Fig. 7 *Admissibility boundaries of wind generation for* ***(a)*** Case 1, ***(b)*** Case 2

*G*2 is used at peak hours to satisfy the remaining load and maximising admissibility boundaries of the OWF output.

Case 2: In this case, the robust day-ahead scheduling problem is calculated to examine the impact of the multi-terminal VSC-HVDC system on the admissibility boundaries of the OWF output. Table 3 shows the UC and ED results; also, this table shows the difference between cases 1 and 2 in UC and ED results. Compared with case 1, the output of inexpensive unit *G*1 is increased in peak hours to supply system loads, since the DC transmission system decreases transmission congestion. As can be seen in Fig. 5, in this test system, two transmission lines are existing, i.e. loop 2–1–4–2 and 2–3–4–5–6–2, and once the multi-terminal VSC-HVDC system is installed in this system, the loop 2–1–4–2 and 2–3–4–5–6–2 will be relaxed, which caused better results. For instance, as shown in Table 3, by hosted multi-terminal VSC-HVDC system, the flow of lines 3–6, 4–5, and 5–6 in the loop 2–3–4–5–6–2 can be raised without affecting the flow on other lines. In fact, the HVDC transmission lines can transfer additional power (compared to the HVAC line 1–2 flow and line 5–6 in case 1) from bus 1 to bus 2 and from bus 5 to bus 6 which results in the mitigation of congestion on lines 1–4, 2–4, and 4–5 and the additional dispatch of the OWF unit. Consequently, it is not necessary to turn on and dispatched the more fast-ramping unit G2, at highest output, just for load supplying at peak hours. For this reason, as shown in Table 3, utilisation of up/down-ramping of thermal unit G2 is more increased with respect to case 1 in order to compensate the uncertainty of OWF output at bus 1.

To study the influence of multi-terminal VSC-HVDC system, admissibility boundaries under multi-terminal VSC-HVDC system are commutated and shown in Fig. 7*b*. Here, *case* 1 is considered as the base case. Obviously, case 2 with *multi-terminal VSC-HVDC system* has the largest admissible region, accordingly, as can be seen in Fig. 7*b*, the admissibility boundaries of the OWF output in this case are increased by 96.4% from 0.4 to 11.1%. This result evidently indicates that, the hosted multi-terminal VSC-HVDC system to eliminate system congestion and maximise the size of admissible regions of the OWF outputs is comparable with the conventional HVAC systems.

Moreover, in case 1 where unit *G*2 is the only flexible option that follows the OWF output uncertainty, as can be seen in Table 3, the fast-ramping unit is committed to provide a quick ramp capacity of 20 MW/(10 min) at hours 13–15 and 19–20 when there is an hourly OWF output decrease and increase, respectively. However, unit *G*2 is more expansive than unit *G*1 in this system; accordingly, the unit *G*2 is turned off when the ramping flexibility is not required. The additional dispatch of expensive quick-ramping unit *G*2 at these hours would increase system operation costs, and as a result, would decrease the admissibility boundaries

Table 3 Hourly scheduling of the thermal units for HVAC/DC systems

	HVAC (α^{max} = 0.004)		HVDC (α^{max} = 0.111)	
	*G*1	*G*2	*G*1	*G*2
1	0.704	0.158	0.862	0.000
2	0.722	0.100	0.822	0.000
3	0.777	0.000	0.777	0.000
4	1.187	0.000	1.187	0.000
5	1.461	0.000	1.461	0.000
6	1.495	0.000	1.495	0.000
7	1.554	0.000	1.554	0.000
8	1.696	0.000	1.696	0.000
9	1.778	0.000	1.778	0.000
10	1.480	0.000	1.480	0.000
11	1.326	0.100	1.326	0.100
12	1.691	0.100	1.691	0.100
13	1.832	0.100	1.732	0.200
14	1.586	0.100	1.486	0.200
15	1.565	0.123	1.489	0.200
16	1.520	0.188	1.543	0.165
17	1.480	0.190	1.495	0.175
18	1.457	0.110	1.457	0.110
19	1.254	0.106	1.160	0.200
20	1.214	0.100	1.114	0.200
21	1.463	0.100	1.463	0.100
22	1.207	0.100	1.307	0.000
23	0.759	0.100	0.859	0.000
24	0.926	0.100	1.026	0.000

Table 4 HVAC/HVDC line flow at hour 19

Line (from bus to bus)	HVAC	HVDC
1–2	−0.03	−0.04
1–4	−0.86	−0.85
2–3	−0.57	−0.57
2–4	−0.955	−0.95
3–6	−0.058	−0.065
4–5	−0.776	−0.791
5–6	0.233	0.248

of OWF uncertainty. Also, the total dispatched ramping of thermal units in cases 1 and 2 are 5.5 and 6.1 p.u., respectively. The total dispatched ramping is the p.u. ramped over total scheduling horizon, which indicates the variations in the thermal power dispatch to compensate the hourly OWF output uncertainty.

In case 2, thermal unit G2 carries out more ramping up/down than its in case 1; so, the total dispatched ramping of thermal units in this case, i.e. 6.1 p.u., is more increased than its in case 1, i.e. 5.5 p.u. These results demonstrate that lack of flexible ramping up/down capability and transmission congestion in this system would raise the system production cost in terms of a lower admissibility boundaries of the OWF output. Also, the results in this case suggest that the multi-terminal VSC-HVDC system provide a more flexible resource and a better option when compared with fast-ramping unit, as it yields lower transmission congestion and more dispatch of the OWF unit which avoids committing expensive quick-ramping unit during peak hours, just for load supplying.

5.2 Modified IEEE 118-bus test system with the OWF integration

In this subsection, the OWF integration is studied using a modified IEEE 118-bus test system which is a sample of large-scale systems [28]. The parameters of transmission network, load profiles, and thermal units are given in [21]. Three OWFs are added to buses 23, 69, and 113. The output profile of the OWFs located at these buses follow the same pattern as that of the six-bus test system, which are

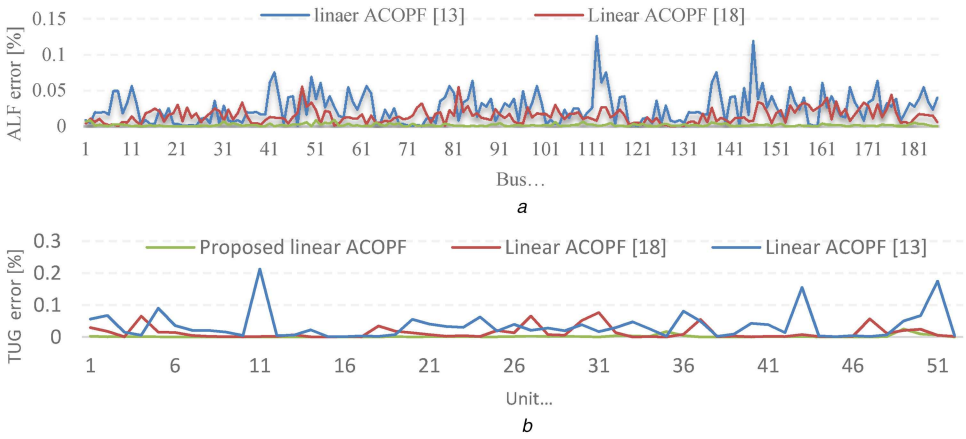

Fig. 8 *Comparison of calculation errors for proposed linear ACOPF model and other models in [13, 18]*
(a) ALF, ***(b)*** TUG

Table 5 α^{max} for the IEEE-118 bus system under different AC OPF models

Grid	ACOPF (MINLP)	Proposed LACOPF (MILP)	LACOPF [23] (MILP)	LACOPF [20] (MILP)
	α^{max}	α^{max}	α^{max}	α^{max}
No. of HVDC grid	0.049	0.050	0.056	0.061
multi-terminal VSC-based HVDC grid	0.147	0.150	0.158	0.166
time (min)	174	23	77	46

scaled by a factor of 6. However, the line flow limits for a few lines are reduced to 100 MW to enforce the system congestion in the simulations. Multi-terminal VSC-HVDC systems are set up at buses with OWFs and the congested areas follow the same capacity and parameters of the previous six-bus test system. The three cases, cases 1 and 2 were studied in the previous system, are examined for this system as well. The results for this test system are consistent with those of the previous system. The following cases are tested in this part.

In case 1, the robust day-ahead scheduling without multi-terminal VSC-HVDC system is solved in order to increase the robustness of the objective function. In case 2, the HVAC lines in case 1 are replaced in some areas with the multi-terminal VSC-HVDC system and the same parameters as it in pervious test system is considered. In case 3, comparison of the proposed linear ACOPF and linear ACOPF proposed in [20, 23] with full ACOPF model with (without) terminal VSC-HVDC system model has been performed.

These multi-terminal VSC-HVDC system are installed in the congested areas based on the robust day-ahead scheduling results obtained in case 1. According to the above-mentioned conditions, the simulations are done and the following results are achieved.

Case 1: It is assumed that the forecasted wind power generation is 100% of its installed capacity for all of the OWFs. The TC of TUG is equal to $TC_b = 0.885$ M$. At this condition, the maximum radius of OWF uncertainty, i.e. α^{max}, is 5%.

Case 2: In this case, the AC transmission lines in the congested areas are replaced with multi-terminal VSC-HVDC system which results in an α^{max} of 15% for $TC_b = 0.885$ M$. The lower α^{max} in case 1 is mainly due to the congestion of HVAC lines at peak hours which causes the commitment of expensive units with lower flexible up/down-ramping. Hosting the HVDC transmission lines, similar to the previous test system, caused decrease in the transmission congestion of HVAC transmission lines; so, the maximum admissibility boundaries of the OWF output uncertainty are increased by 66.6% from 5 to 15%. Also, it is observed from the obtained results that by decreasing transmission congestion, the participation of the OWF in energy supplying increases, whereas in contrary, the participation of expensive thermal generation units are decreased, which shows more system flexibility for implementing multi-terminal VSC-HVDC system in large-scale power systems.

Case 3: The simulations are performed to obtain the active line flow (ALF) and the TUG using the proposed linear ACOPF model and the linear ACOPF models in [20, 23]. Furthermore, we consider the multi-terminal VSC-based HVDC grid simultaneously at all of the OPF models. Considering the full ACOPF results as the reference, the calculation errors are given by:

$$\Delta_{nm}^{LAC} = \left| P_{nm}^{AC} - P_{nm}^{LAC} \right| \tag{9a}$$

$$\Delta_{g}^{LAC} = \left| P_{g}^{AC} - P_{g}^{LAC} \right| \tag{9b}$$

Equation (9a) is the calculation error of the active power flow in line (n, m) which is obtained from all models of the linear ACOPF model proposed in this paper and in [20, 23], and the full ACOPF solution. Also, (9b) is the calculation error of the unit generations from thermal unit g similar to (9a). As can be seen in Fig. 8*a*, the maximum value of the error calculated for Δ_{nm}^{LAC}, for our proposed linear ACOPF model and the linear ACOPF models in [20, 23], are 0.009, 0.126, and 0.055 p.u., respectively. Similarly, the mean value of the error calculated for Δ_{nm}^{LAC}, for these models are 0.001, 0.025, and 0.015 p.u., respectively. Also, in Fig.8*b*, the maximum value of Δ_{g}^{LAC} for our proposed linear ACOPF model and the linear ACOPF models in [20, 23] are 0.025, 0.076, and 0.212 p.u., respectively. In addition, the mean value of Δ_{g}^{LAC} for these models are 0.001, 0.013, and 0.034 p.u., respectively. These results indicate that the ALF through the lines and the TUG of thermal units are obtained by our proposed linear ACOPF model provides more precise results for large-scale systems. Also, in this case, the α^{max} obtained from the full ACOPF model with (without) multi-terminal VSC-based HVDC grid are 5 and 15%, respectively. The same results are approximately obtained by our proposed linear ACOPF model with (without) linear multi-terminal VSC-based HVDC lines. As shown in Table 5, the α^{max} obtained by day-ahead scheduling problem based on the AC-OPF model, with (without) multi-terminal VSC-based HVDC lines, are much closer to our proposed linear ACOPF model than other models, it is showing the efficiency of the proposed linear ACOPF model for large-scale systems.

The elapsed time to solve the day-ahead scheduling problem with multi-terminal VSC-based HVDC grid by the full ACOPF approach is ~174 min and by proposed linear ACOPF is <23 min which is lower than two other models in [20, 23]. Finally, as the results show, our proposed linear ACOPF model is more efficient for the day-ahead scheduling problem with (without) multi-terminal VSC-based HVDC grid and has a reasonable run.

6 Conclusions

This paper presents a robust day-ahead scheduling problem with multi-terminal VSC-HVDC grid model assuming a high penetration of the OWFs output, based on an MILP approach. The MILP approach uses a linear model of AC OPF with linear multi-terminal VSC-HVDC grid model, which allows the voltage and reactive power to be considered directly once designing the real-world power flow. The proposed linear ACOPF model approximates the AC network more accurately, and therefore provides more realistic operation results. Simulation results for the IEEE 118-bus system show that the proposed linear ACOPF model can be applied to solve large-scale day-ahead scheduling problems with more accurate approximation of the AC network.

The proposed robust day-ahead scheduling problem simultaneously coordinates the scheduling of onshore HVAC with offshore HVDC to have maximum admissibility boundaries of the OWFs output uncertainty for large-scale integration of them. In addition, the multi-terminal VSC-HVDC network can mitigate onshore HVAC network congestion. Numerical results demonstrated that by coordination of the HVAC grid and HVDC grid with increased grid side flexibility, the maximum admissibility boundaries of the OWFs output values are increased.

Besides, in this paper, a non-probabilistic and non-possibilistic method is utilised for handling the uncertainties associated with the OWFs output volatility. The proposed uncertainty model is computationally efficient and does not require the probability density function of the wind speed. Also, the proposed decision-making framework finds the optimal decision variables in a way that they remain robust against the considered uncertainties. The numerical results indicated the well functioning of the proposed uncertainty model. In order to obtain tractable problem and accelerate the execution time, the proposed model has been formulated based on the proposed BD technique in the large-scale system.

In this work, the multi-terminal VSC-HVDC system has been used as the main resource of grid side flexibility. However, in addition to this type of existing flexible resource, there are other grid side sources of flexibility which also need to be investigated. The main alternative grid side source of flexibility include transmission switching and flexible AC transmission system devices. As a future work, these flexibility resources can be integrated into the proposed mathematical model by adding the corresponding constraints, relationships, and parameters. Their effects on the wind power utilisation can then be assessed. The most important challenge is how to tackle the intensive computational requirements, especially when applying the transmission switching action in real power systems. This will rely on further improvement of solution strategy.

7 References

[1] Ergun, H., Van Hertem, D., Belmans, R.: 'Transmission system topology optimization for large-scale offshore wind integration', *IEEE Trans. Sustain. Energy*, 2012, **3**, (4), pp. 908–917

[2] Bresesti, P., Kling, W.L., Hendriks, R.L., *et al.*: 'HVDC connection of offshore wind farms to the transmission system', *IEEE Trans. Energy Convers.*, 2007, **22**, (1), pp. 37–43

[3] Lotfjou, A., Shahidehpour, M., Fu, Y.: 'Hourly scheduling of DC transmission lines in SCUC with voltage source converters', *IEEE Trans. Power Deliv.*, 2011, **26**, (2), pp. 650–660

[4] Rabiee, A., Soroudi, A., Keane, A.: 'Information gap decision theory based OPF with HVDC connected wind farms', *IEEE Trans. Power Syst.*, 2015, **30**, (6), pp. 3396–3406

[5] Chaudhary, S.K., Teodorescu, R., Rodriguez, P., *et al.*: 'Negative sequence current control in wind power plants with VSC-HVDC connection', *IEEE Trans. Sustain. Energy*, 2012, **3**, (3), pp. 535–544

[6] Bernal-Perez, S., Ano-Villalba, S., Blasco-Gimenez, R., *et al.*: 'Efficiency and fault ride-through performance of a diode-rectifier-and VSC-inverter-based HVDC link for offshore wind farms', *IEEE Trans. Ind. Electron.*, 2013, **60**, (6), pp. 2401–2409

[7] Xu, L., Yao, L.: 'DC voltage control and power dispatch of a multi-terminal HVDC system for integrating large offshore wind farms', *IET Renew. Power Gener.*, 2011, **5**, (3), pp. 223–233

[8] Muyeen, S., Takahashi, R., Tamura, J.: 'Operation and control of HVDC-connected offshore wind farm', *IEEE Trans. Sustain. Energy*, 2010, **1**, (1), pp. 30–37

[9] Fu, Y., Wang, C., Tian, W., *et al.*: 'Integration of large-scale offshore wind energy via VSC-HVDC in day-ahead scheduling', *IEEE Trans. Sustain. Energy*, 2016, **7**, (2), pp. 535–545

[10] Baradar, M., Ghandhari, M.: 'A multi-option unified power flow approach for hybrid AC/DC grids incorporating multi-terminal VSC-HVDC', *IEEE Trans. Power Syst.*, 2013, **28**, (3), pp. 2376–2383

[11] Mehrasa, M., Pouresmaeil, E., Zabihi, S., *et al.*: 'A multi-loop control technique for the stable operation of modular multilevel converters in HVDC transmission systems', *Int. J. Electr. Power Energy Syst.*, 2018, **96**, pp. 194–207

[12] Mehrasa, M., Pouresmaeil, E., Zabihi, S., *et al.*: 'Dynamic model, control and stability analysis of MMC in HVDC transmission systems', *IEEE Trans. Power Deliv.*, 2017, **32**, (3), pp. 1471–1482

[13] Mehrasa, M., Hosseini, S., Taheri, S., *et al.*: 'Dynamic performance control of modular multilevel converters in HVDC transmission systems'. Electrical Power and Energy Conf. (EPEC), 2016 IEEE, 2016, pp. 1–6

[14] Iggland, E., Wiget, R., Chatzivasileiadis, S., *et al.*: 'Multi-area DC-OPF for HVAC and HVDC grids', *IEEE Trans. Power Syst.*, 2015, **30**, (5), pp. 2450–2459

[15] Aghaei, J., Nikoobakht, A., Siano, P., *et al.*: 'Exploring the reliability effects on the short term AC security-constrained unit commitment: a stochastic evaluation', *Energy*, 2016, **114**, pp. 1016–1032

[16] Lin, W., Wen, J., Cheng, S., *et al.*: 'An investigation on the active power variations of wind farms'. Industry Applications Society Annual Meeting (IAS), 2011 IEEE, 2011, pp. 1–8

[17] Aien, M., Hajebrahimi, A., Fotuhi-Firuzabad, M.: 'A comprehensive review on uncertainty modeling techniques in power system studies', *Renew. Sust. Energy Rev.*, 2016, **57**, pp. 1077–1089

[18] Siahkali, H., Vakilian, M.: 'Fuzzy generation scheduling for a generation company (GenCo) with large scale wind farms', *Energy Convers. Manage.*, 2010, **51**, (10), pp. 1947–1957

[19] Martinez-Mares, A., Fuerte-Esquivel, C.R.: 'A robust optimization approach for the interdependency analysis of integrated energy systems considering wind power uncertainty', *IEEE Trans. Power Syst.*, 2013, **28**, (4), pp. 3964–3976

[20] Nikoobakht, A., Mardaneh, M., Aghaei, J., *et al.*: 'Flexible power system operation accommodating uncertain wind power generation using transmission topology control: an improved linearised AC SCUC model', *IET Gener. Transm. Distrib.*, 2017, **11**, (1), pp. 142–153

[21] Nikoobakht, A., Aghaei, J.: 'IGDT-based robust optimal utilisation of wind power generation using coordinated flexibility resources', *IET Renew. Power Gener.*, 2016, **11**, (2), pp. 264–277

[22] Nikoobakht, A., Aghaei, J., Mardaneh, M.: 'Managing the risk of uncertain wind power generation in flexible power systems using information gap decision theory', *Energy*, 2016, **114**, pp. 846–861

[23] Akbari, T., Bina, M.T.: 'Linear approximated formulation of AC optimal power flow using binary discretisation', *IET Gener. Transm. Distrib.*, 2016, **10**, (5), pp. 1117–1123

[24] Misener, R., Floudas, C.: 'Piecewise-linear approximations of multidimensional functions', *J. Optim. Theory Appl.*, 2010, **145**, (1), pp. 120–147

[25] Beale, E., Forrest, J.J.: 'Global optimization using special ordered sets', *Math. Program.*, 1976, **10**, (1), pp. 52–69

[26] Gurobi Optimization: *'Gurobi optimizer reference manual'*. [Online]. Available at http://www.gurobi.com

[27] Shahidehopour, M., Fu, Y.: 'Benders decomposition: applying Benders decomposition to power systems', *IEEE Power Energy Mag.*, 2005, **3**, (2), pp. 20–21

[28] IIT Power Group, 2003. Available at http://motor.ece.iit.edu/data/JEAS_IEEE118.doc